RICE UNIVERSITY

DETERMINATION OF THE FLOW FIELD IN A CONFINED VORTEX CHAMBER

by

Burkhard Schulz-Jander

A THESIS

SUBMITTED TO THE FACULTY

IN PARTIAL FULFILLMENT OF THE

REQUIREMENTS FOR THE DEGREE OF

MASTER OF SCIENCE

Thesis Director's Signature:

Herbert Bukmann

Houston, Texas

May, 1963

ABSTRACT

The flow field in a cylindrical vortex chamber was investigated experimentally. The tangetial velocity distribution was found to resemble a solid body rotation in the outer region, and a vortex flow in the center. A theory derived for the pressure and velocity distributions agreed very well with experiments. Close to the flat walls a secondary flow towards the center of the vortex was detected, which contributed to most of the mass flow through the chamber.

ACKNOWLEDGEMENT

This investigation was sponsored in part by the Shell Company's Foundation Incorporated.

The author wishes to express his appreciation to Dr. Herbert Beckmann for his guidance in this work.

TABLE OF CONTENTS

INTRODUCTION

A vortex flow is created in a cylindrical chamber by tangential injection of a fluid at the outer edge and the subsequent discharge of this fluid through an orifice or nozzle in the center of one of the lateral walls of the chamber. Such a flow has recently become of interest as a result of its application to the stabilization of electric arcs in plasmajet generators. To advance the understanding of this type of flow, such a configuration was investigated with a fluid of constant density. There exist a number of analytical and experimental studies[1-6]* the majority of which are concerned with the temperature separation effect, in which there is a stream of hot air near the outer wall and one of cold air in the center region; this is commonly referred to as the Ranque-Hilsch[5,6] effect. These temperature distributions were not investigated since the high heating rates applied in a plasmajet generator would quite significantly change the flow pattern. The effect of wall friction, however, seemed to merit investigation. J. E. Lay,[3] who derives a hodograph equation for potential vortex flow, states that potential flow is maintained only in a small region at the entrance and that viscosity effects soon start to significantly influence the flow behavior. Even for air, with its relatively low

---

* Superscript numbers refer to references listed on page 21.

viscosity, Lay's experiments indicated that the effects of viscosity were quite significant.

In this study the effect of wall friction on the velocity and pressure distributions will be investigated analytically and experimentally, using water as an incompressible fluid with a relatively high viscosity.

LIST OF SYMBOLS

A	surface area
C	integration constant in equation (20)
C_f	friction coefficient
C_p	pressure coefficient
K_1	characteristic constant of the flow field according to equation (23)
$\mathring{m}$	mass flow rate through the chamber
p	static pressure
$\not{p}$	recorded static pressure difference $p_o - p$
q	stagnation pressure [inches of water pressure]
r	radial distance from the vortex center
v	tangential velocity component
w	radial velocity component
α	angle between the flow direction and the radius vector $\vec{r}$ [°]
ν	kinematic viscosity of the fluid
ρ	density of the fluid
τ	friction force per unit area

Subscripts :

o	properties at the cylindrical wall
$*$	properties at the inlet pipe

2. THEORETICAL APPROACH

2.1 General Remarks

In a right circular cylinder a fluid was tangentially injected at the outer cylindrical wall. The fluid left the chamber through a nozzle in the center of one of the lateral circular plates. The energy loss due to friction along the cylindrical wall will be evaluated in part 2.2 of this chapter. The subsequent loss of moment of momentum along the two flat lateral walls will be considered in section 2.3; the equation for the velocity distribution obtained thereby will then be used to acquire the static pressure distribution in the chamber (part 2.4).

2.2 Evaluation of the Frictional Loss along the Outer Cylindrical Wall

The fluid entering the vortex chamber (Fig. 1) through a circular pipe of crosssection A_* with a velocity v_* loses part of its energy due to friction at the circular wall. The energy loss per unit time is given by

$$\dot{m}\frac{v_*^2}{2} - \dot{m}\frac{v_o^2}{2} = \tau A_o v_o \qquad (1)$$

where $\dot{m}$ is the mass flow rate

$$\dot{m} = \rho v_* A_* \qquad (2)$$

A_o is the circular wall area, v_o the velocity of the fluid close to

that wall, and τ being the friction force per unit area, which can be evaluated by the relation

$$\tau = C_f \left(\tfrac{1}{2} \rho v_o^2 \right) \qquad (3)$$

The substitution of the equation (2) and (3) into the energy balance (1) yields, after some rearranging, for a fluid with constant density

$$v_o^2 = \frac{1}{\left[1 + C_f \left(\frac{A_o}{A_*} \right) \left(\frac{v_o}{v_*} \right) \right]} \; v_*^2 \qquad (4)$$

In the case of turbulent flow along a smooth flat plate, Schlichting[9] gives the following relation for C_f

$$C_f = 0.074 \; Re^{-0.2} \qquad (5)$$

where the Reynolds Number will be evaluated with $(2\pi r_o)$ as a characteristic length and v_o as the determining velocity. Thus

$$Re_o = \frac{2\pi r_o v_o}{\nu} \; .$$

This expression can be written as

$$Re_o = \frac{2\pi r_o v_*}{\nu} \left(\frac{v_o}{v_*} \right) \qquad (6)$$

$$Re_o = Re_{*o} \left(\frac{v_o}{v_*} \right)$$

where Re_{*o} depends only on the known geometry and inlet velocity.

Using equation (5) and (6) to eliminate C_f from (4) yields

$$v_o^2 = \frac{1}{\left[1 + 0.074 \frac{A_o}{A_*} \, Re_{*o}^{-0.2} \left(\frac{v_o}{v_*}\right)^{0.8}\right]} \, v_*^2 \qquad (7)$$

It can be seen that in equation (7) the variables v_o and v_* cannot be separated. But a reasonable conjecture for the ratio (v_o/v_*) will soon converge on the right result.

For the configuration experimentally investigated in section 3 with

$$\frac{A_o}{A_*} = 468$$

$$v_* = 2.15 \text{ [m/sec]}$$

$$Re_{*o} = 3.32 \times 10^6$$

it is found from equation (7) that

$$v_o = 0.68 \, v_* \qquad (8)$$

This agrees very well with measurements, which indicated that

$$\left(\frac{v_o}{v_*}\right)_{test} = 0.697$$

2.3 Determination of the Velocity Distribution in the Vortex Chamber

For the non-viscous case the flow in the investigated chamber can be represented by a superposition of a vortex and a source or sink flow. Vogelpohl[7] has given a solution of the Navier-Stokes-Equations for a vortex-source between two parallel walls. Even though this theory can also be applied to a vortex-sink flow, the result in terms of Weierstrass $\wp$-functions is inconvenient for further use. Since this solution neglects all velocities perpendicular to the walls, it does not give any information about the boundary layer change; thus all velocity profiles are similar to the incoming distributuion of the incoming flow.

Because of these shortcomings in Vogelpohl's solution, a two-dimensional approach which was first suggested by Pfleiderer[8] will be used here.

Newton's fundamental theorem of the mechanics of discrete particles states that the change of moment of momentum around a point or axis is equal to the moment of external forces

$$\frac{d}{dt} \left(m \; \vec{v} \times \vec{r} \right) = \vec{M} \qquad (9)$$

or

$$\left(\vec{v} \times \vec{r} \right) \frac{dm}{dt} + m \frac{d}{dt} \left(\vec{v} \times \vec{r} \right) = \vec{M} \qquad (10)$$

For steady state, where $\left(\vec{v} \times \vec{r} \right)$ does not depend on time, and with

the mass flow rate

$$\dot{m} = \frac{d\,m}{d\,t} \qquad (11)$$

this reduces to

$$\dot{m}\,(\vec{v} \times \vec{r}) = \vec{M} \quad .$$

For a continuous function and $\vec{v}$ perpendicular to $\vec{r}$ this can be written as

$$\dot{m}\,d\,(v\,r) = d\,M \qquad (12)$$

The wall friction at the two parallel walls will be considered as the only external force experienced by the fluid. With the surface area

$$2\,dA = 4\,\pi\,r\,dr \qquad (13)$$

the frictional moment can be expressed as

$$dM = 4\,\pi\,r^2\,dr\,\tau \qquad (14)$$

The Reynolds number occuring in equation (5) for the friction coefficient will be evaluated by the expression

$$Re = \frac{2\,\pi\,r_o\,v}{\nu} = Re_o\,\frac{v}{v_o} \qquad (15)$$

where

$$Re_o = \frac{2\,\pi\,r_o\,v_o}{\nu} \qquad (16)$$

The use of expression (13) through (15) together with the definitions (3) and (5) in equation (12) yields

$$\frac{d\,(v\,r)}{(v\,r)^{1.8}} = K_1\,r^{0.2}\,dr \qquad (18)$$

where K_1 is the constant

$$K_1 = 0.074 \left(2 \pi \right) \frac{\rho}{m_o} \left(\frac{v_o}{Re_o} \right)^{0.2} \qquad (19)$$

Equation (18) becomes, upon integration

$$- 1.25 \left(v\, r \right)^{-0.8} = \frac{K_1}{1.2} r^{1.2} + C_1 \qquad (20)$$

The integration constant C_1 is evaluated such that for $r = r_o$ the velocity v becomes v_o. Then

$$C_1 = -1.25 \left(v_o\, r_o \right)^{-0.8} - \frac{K_1}{1.2} r_o^{1.2} \qquad (21)$$

Combining equation (20) , (21) and (3) leads, after rearanging to the expression

$$\frac{v_o}{v} = \frac{r}{r_o} \left[1 + K \left\{ 1 - \left(\frac{r}{r_o} \right)^{1.2} \right\} \right]^{\frac{5}{4}} \qquad (22)$$

where

$$K = 2.0433 \left(\frac{v_o}{v_*} \right) \left(\frac{r_o}{r_*} \right)^2 C_{f_o} \qquad (23)$$

with

$$C_{f_o} = 0.074 \; Re_o^{-0.2} \qquad (24)$$

for smooth surfaces.

It can be seen that for the special case of no friction, or $K = 0$, equation (22) reduces to $v \cdot r$ = constant, which is the well-known relation for a perfect vortex.

The function (v/v_o) was plotted for various values of K in Figure 3. For the configuration, which was tested experimentally, where

$$\frac{r_o}{r_*} = 19$$

$$\frac{v_o}{v_*} = 0.697$$

$$Re_o = 2.18 \times 10^6$$

the constant K becomes

$$K = 2.10 \qquad (25)$$

2.4 Determination of the Pressure Distribution

The inviscid relation

$$\frac{dp}{dr} = \rho \frac{v^2}{r} \qquad (26)$$

may be used to calculate the pressure distribution from the velocity distribution determined in the previous section. Equation (22) can be solved for v as

$$v = \frac{v_o}{\left(\frac{r}{r_o}\right)} \left[1 + K \left\{ 1 - \left(\frac{r}{r_o} \right)^{1.2} \right\} \right]^{-\frac{5}{4}}$$

Realizing also that $dr = r_o \, d(r/r_o)$, equation (26) becomes

$$\frac{d\left(\frac{p}{\frac{1}{2}\rho v_o^2}\right)}{d\left(\frac{r}{r_o}\right)} = \frac{2}{\left[1 + K\left\{1 - \left(\frac{r}{r_o}\right)^{1.2}\right\}\right]^{2.5}\left(\frac{r}{r_o}\right)^3} \qquad (27)$$

This expression was integrated numerically on the IBM 1620 Data Processing System; the computation scheme is illustrated in the appendix. The resulting pressure distribution

$$C_p = \frac{p - p_o}{\frac{1}{2}\rho v_o^2} = fn \; (r/r_o)$$

is plotted in Figure 5 for several values of the constant K according to equation (23). The boundary conditions are chosen such that at $r = r_o$ the pressure is equal to p_o.

For the frictionless case K = 0 a complete integration of (27) can be performed which results in the relation

$$C_{p_{vor}} = \left[1 - \left(\frac{r_o}{r}\right)^2\right] \qquad (29)$$

For a fluid rotating like a solid body, a similar analysis leads to the expression

$$C_{p_{rot}} = \left[\left(\frac{r}{r_o}\right)^2 - 1\right] \qquad (30)$$

which was denoted by the dashed line in Figure 5 . It is seen that for constants K about equal to 2 the pressure distribution of a vor-

tex with friction does not differ much from that of a solid rotating body for radius ratios larger than 0.7 .

Equation (29) was used to evaluate the error resulting from the numerical integration of expression (27) . Since the integration began at $r = r_o$, the largest deviations from the true values were expected for small radii. For $K = 0$ and $r/r_o = 0.2$, the error obtained was found to be about one quarter of one per cent.

3. EXPERIMENTAL PART

3.1 Test Stand Description

A cylindrical vortex chamber was constructed of plexiglas. Its diameter was 9.5 inches and its height 3.06 inches (Figure 1). The inlet jet entered tangentially into the cylindrical wall having an equal distance from both flat sides. The exit hole in the center of the bottom flat plate was designed as a simple converging nozzle. Both exit and inlet diameters were 1/2 inch. Water was supplied and recycled by a pump with a constant mass flow rate of 6.45 gallons per minute, which was indicated by a flow meter. A pressure vessel was put in line between the pump and the vortex chamber in order to ensure a constant inlet pressure and to eliminate fluctuations in the flow rate. By means of this tank which was connected to a compressed air line, the static pressure in the chamber could be adjusted arbitrarily. This became necessary to eliminate a core of air in the center of the vortex. The air core appeared at the start of the tests as well as later when it had been regenerated from air which had been in solution in the water. This core and the free surface inside the vortex due to the air core were eliminated by raising the pressure in the center of the vortex above one atmosphere and draining the air off through a hole opposite the exit nozzle . At various positions of the chamber, holes of 1/16 inch diameter were drilled through the walls. They were used to measure wall pressures as well as to insert probes for static and stagnation

pressure measurements. Because of the interference of any probes with the flow, a fact which was also observed by Holman[1], they had to be very small and were made from 0.025 inch diameter stainless steel pipes. The friction inside these pipes resulted in extremely long response times until equilibrium was achieved for pressure readings.

Four different pressure readings were taken simultaneously. The pressure gages M_1 and M_2 showed the pressure in the vessel and at the inlet of the vortex chamber; both were referred to the atmospheric pressure. M_3 was a U-type manometer filled with mercury which read the pressure difference between the inlet and the outlet pipe of the chamber. A change or oscillation in this pressure was an indication of the degree of interference of probes inserted into the chamber. The manometer M_4 was used to measure the pressure at any desired position in the flow field or at the walls. Since water was used as the indicating fluid, a water trap had to be built such that no fluid from the chamber could flow into the U-pipe. These traps also had to be built such that the fluid levels inside could be kept at equal heights. Because of the small range of this manometer the reference pressure had to be changed according to the requirements, though in most cases it was referred to the static pressure along the outer chamber wall.

A schematic drawing of the test stand is given in Figure 2.

3.2 Test Procedure

Static and dynamic pressure readings were taken for twelve different radial distances r/r_o at eleven axial positions between the two flat walls. Since extremely small probes had to be used for minimum interference, it was not possible to measure the static and stagnation pressure simultaneously with a Prandtl tube. Thus these measurements were taken successively with two different probes. They could only be exchanged after the flow had been turned off and the water had been drained from the chamber. For this reason extreme care had to be taken to ensure a constant mass flow rate and reference pressure for all tests. For each position at least three readings were taken from each probe in order to reduce errors. These errors usually resulted from the failure to align the probes in the proper flow direction. To accomplish this alignment as well as to measure the direction of the flow, a small tuft was fastened to the back of the probes. The direction of this thread could easily be read through the plexiglas wall by means of a protractor. The injection of dyes to accomplish the same failed because the turbulence in the chamber together with the disturbance from the inserted probe caused the dye to spread out and mix with the water at a high rate. The insertion of solid particles in connection with a photographic recording system was not successful because of the difficulties of properly locating those particles. The method of using threads gave rise to several errors:

1. The connection between the thread and the probe had a cer-

tain stiffness such that the position of the probe influenced the indicated direction. This fact could easily be seen by turning the probe by several degrees. Within a range of about two degrees the thread would follow the rotation of the probe. Only at larger angles it would adjust itself to a different position. This error influenced mainly the measurements at large radii, where the streamlines were found to be very nearly circles.

2. Another type of error resulted from the drag of the thread in connection with the spiralic paths of the water particles. Especially in regions of large curvature of the streamlines this force pulled the thread towards the center of the vortex. For this reason the computed radial velocity components were rather inaccurate, a fact which will be discussed in the next chapter.

The probes were inserted into the chamber from both sides such that they never extended into the flow more than half the height of the chamber. This kept the total drag force reasonably small and in most cases prevented the very thin probes from oscillations. The drag became significant, however, in the region close to the center of the vortex, where the velocities were already very large. Only a few points close to the wall could be measured in this region. At the bottom plate no measurements could be taken in this area because the exit nozzle prevented the insertion of any probes.

A special phenomenon was encountered in the region where the average tangential velocity according to equation (22) had its minimum. Probes which were inserted in this area caused the center of the vortex to move on circles around the geometric center of the chamber. No valid results could be obtained under such conditions. Experiments with a different chamber with a larger height to diameter ratio of ($h/2r_o$) = 0.525 had to be discontinued since this effect became too serious.

Static pressure readings were also taken along all walls of the chamber. They did not pose any problems.

3.3 Test Results

The tangential components v of the measured velocity profiles between the two flat walls at constant radius ratios are shown in Figures 7-9. It is seen that the first profile of r/r_o = 0.92 still indicates some non-uniformity due to the inlet jet which has spread out but still shows two distinct maxima. In the next position closer to the center this starting condition has already faded out, the vortex flow is established across the entire width of the chamber. The average tangential velocities decrease up to a radius ratio of r/r_o = 0.6 and increase very rapidly from there towards the center. In Figure 4 the measured average velocities are plotted versus radial position. It is seen that at large radii the motion resembles a solid body rotation, where v is proportional to r and closer to the center it changes to a vortex where $v \cdot r$ = const. The theory

derived in section 2.3 (Figure 4) is seen to agree very well with these results.

The radial velocity components w are plotted in Figures (10-12). Because of the inaccuracy of their determination, the profiles shown represent only qualitative results. It is seen that the largest amount of radial velocity occurs always close to the wall. One also sees in the region where r/r_o = 0.75...0.60 and h/h_o = 0.4...0.6, the radial velocity goes to zero. This means that there exists a ring of fluid, which rotates like a solid body and does not take part in the main flow through the chamber.

The recorded pressures are shown in Figure 6. The free stream pressures were obtained by averaging the static pressure readings for all axial positions h/h_o from 0.8 to 0.2 at constant radius. The results show good agreement with the theory derived in section 2.4. The static pressure readings along the walls, however, indicate always higher values. This is not surprising if one realizes that because of the smaller velocity in the boundary layer the centrifugal forces are no more in equilibrium with the forces resulting from the pressure gradient. Thus the particles close to the wall are accelerated towards the center of the vortex and at the same time the wall pressure does not decrease as rapidly as in the free stream. This explains why the largest radial velocities were observed close to the walls. This secondary flow obviously also effects the tangential velocity profiles since they show slightly larger values close to the wall for radial positions from r/r_o = 0.5 to the center.

The theory which was used to obtain the pressure distribution neglects all viscosity effects between the fluid particles and leads to the result that the pressure coefficient C_p becomes ∞ at $r = 0$. The measurements, however, indicate a rather low, but finite value. Thus at a certain radius r_{min} the vortex breaks down and a core is formed which rotates like a solid body. From the analysis in section 2.4 the radius corresponding to the minimum pressure reading in the center of the vortex chamber is found to be

$$r_{min} = 0.038\ r_o$$

Thus in the tested configuration, the diameter of the center core was about 68% of the exit pipe diameter.

Because of the simplifications made in the analysis, this result can, of course, only give an estimate of the actual core size. This method, however, seems more reliable than the direct approach of trying to measure the maximum velocity with the use of probes.

4. CONCLUSION

The experimental investigation of the flow field in a confined vortex chamber showed that for an incompressible medium the flow pattern was mainly determined by the wall friction. An analysis which was based on this fact and which neglected all viscosity effects between the flow particles was found to agree very well with the experiments.

REFERENCES

1. Holman, J. P., and Moore, G. D., "Experimental Study of Vortex Chamber Flow", Transactions of the ASME, Journal of Basic Engineering, December, 1961, pp. 632-636.

2. Savino, J. M. and Ragsdale, R. G., " Some Temperature and Pressure Measurements in Confined Vortex Fields", Transactions of the ASME, Journal of Heat Transfer, February 1961, pp. 33-38.

3. Lay, J. E., " An Experimental and Analytical Study of Vortex-Flow Temperature Separation by Superposition of Spiral and Axial Flows", Transactions of the ASME, Journal of Heat Transfer, August, 1959, pp. 202-222.

4. Hartnett, J. P., and Eckert, E. R. G., "Experimental Study of the Velocity and Temperature Distribution in a High-Velocity Vortex-Type Flow", Transactions of the ASME, May, 1957, pp. 751-758.

5. Ranque, G., "Expériences sur la détente giratoire avec productions simultanées d'un échappement d'air chaud et d'un échappement d'air froid ", Journal de Physique et le Radium, 1933, pp. 112s - 115s.

6. Hilsch, R. " Die Expansion von Gasen im Zentrifugalfeld als Kälteprozess", Zeitschrift für Naturforschung, 1946, pp. 208-214.

7. Vogelpohl, G., "Die Strömung aus einer Wirbelquelle zwischen ebenen Wänden mit Berücksichtigung der Wandreibung", Zeitschrift für angwandte Mathematik und Mechanik, Band 24, Nr. 5 und 6, 1944, pp. 289-293.

8. Pfleiderer, C.,"Untersuchungen an Kreiselradmaschinen," Forschungsarbeiten auf dem Gebiet des Ingenieurwesen, Heft 295, 1927, pp. 84-85.

9. Schlichting, H., Boundary Layer Theory, (4th Ed.) Mc Graw-Hill, New-York, 1960, p. 537.

TEST DATA

	r/r_o = 0.92			r/r_o = 0.837		
h/h_o	q	ϕ	α	q	ϕ	α
.974	3.21	1.13	86.5	2.33	1.38	84.5
.928	3.02	1.30	88.5	2.40	1.51	87.8
.827	3.53	1.41	88.5	2.66	1.54	87.5
.718	4.02	1.61	89.0	2.82	1.53	87.2
.609	3.90	1.60	87.5	2.93	1.55	87.0
.500	3.43	1.31	87.9	3.00	1.58	87.0
.392	3.86	1.56	88.5	2.99	1.54	87.0
.283	4.18	1.68	88.7	2.97	1.58	89.2
.174	3.96	1.55	98.5	2.78	1.53	90.0
.062	3.06	1.21	89.2	2.38	1.48	90.0
.025	3.41	1.16	85.5	2.36	1.36	84.0

	r/r_o = 0.754			r/r_o = 0.672		
h/h_o	q	ϕ	α	q	ϕ	α
.974	1.87	1.63	77.5	1.98	21.3	72.0
.928	2.14	1.72	83.2	2.32	2.38	83.7
.827	2.23	1.78	86.0	2.36	2.32	87.0
.718	2.21	1.76	86.6	2.23	2.17	88.2
.609	2.29	1.94	89.6	2.25	2.15	89.5
.500	2.31	1.81	89.0	2.25	2.15	89.3
.392	2.28	1.89	88.3	2.21	2.12	88.5
.283	2.36	1.84	86.3	2.26	2.10	86.8
.174	2.34	1.79	86.0	2.16	2.08	84.7
.062	2.34	1.80	84.5	2.08	2.10	82.5
.025	1.98	1.68	76.5	2.14	2.14	73.8

	r/r_o = 0.588			r/r_o = 0.506		
h/h_o	q	ϕ	α	q	ϕ	α
.974	1.95	2.53	73.7	2.51	3.34	70.5
.928	2.19	2.59	83.2	2.59	3.46	85.0
.827	2.36	2.70	87.8	2.58	3.43	87.2
.718	2.33	2.94	88.0	2.64	3.45	88.0
.609	*	*	88.1	2.45	3.45	85.5
.500	*	*	87.9	2.41	3.41	86.3
.392	*	*	87.3	2.48	3.44	85.6
.283	*	2.97	88.0	2.76	3.40	85.8
.174	2.62	2.92	87.0	2.77	3.51	84.7
.062	2.34	3.00	81.6	2.63	3.42	82.8
.025	2.18	2.71	72.0	2.54	3.37	72.8

	r/r_o = 0.422			r/r_o = 0.336		
h/h_o	q	ϕ	α	q	ϕ	α
.974	2.86	4.48	64.5	4.29	5.96	66.0
.928	2.88	4.45	81.3	5.02	6.48	82.7
.827	3.07	4.25	81.3	4.83	6.40	83.5
.718	3.03	4.38	83.5	4.56	6.26	83.0
.609	2.91	4.40	81.8	4.11	6.14	82.3
.500	2.82	4.38	82.3	4.00	6.03	83.4
.392	2.91	4.40	84.0	4.02	6.07	84.5
.283	3.05	4.50	84.5	4.25	6.31	85.7
.174	3.15	4.48	82.3	4.71	6.57	84.3
.062	3.19	4.60	81.3	4.64	6.39	86.2
.025	2.88	4.22	73.2	4.44	6.07	70.0

* No valid measurements could be obtained at these positions.

	$r/r_o = 0.248$			$r/r_o = 0.166$		
h/h_o	q	ϕ	α	q	ϕ	α
.974	7.38	10.0	60.0	15.45	19.2	52.0
.928	8.24	10.6	84.0	16.45	20.3	78.8
.827	8.17	10.6	83.0	14.48	18.9	77.7
.718	7.65	10.4	83.5	13.40	18.4	79.0
.609	7.33	10.4	82.8	*	*	*
.500	6.91	10.3	82.7	*	*	*

	$r/r_o = 0.083$			$r/r_o = 0.0415$		
h/h_o	q	ϕ	α	q	ϕ	α
.974	70.06	93.91	45.6	211.0	245.3	54.3
.928	65.38	93.62	67.6	129.7	221.3	46.6
.827	56.26	85.97	71.5	152.5	258.5	41.0

Static pressure readings p at

r/r_o	top wall	bottom wall	mean free stream
0.920	0.54	0.33	1.40
0.837	0.84	0.71	1.55
0.754	1.30	1.21	1.82
0.672	1.70	1.59	2.29
0.588	2.12	2.14	2.83
0.506	2.76	2.78	3.42
0.422	3.60	3.59	4.43
0.336	5.10	5.05	6.24
0.315		5.55	
0.248	7.99		10.34
0.197		11.26	
0.166	14.95		18.68
0.118		27.10	
0.0832	44.10		85.96
0.0526		129.20	258.30
0.000	361.5		

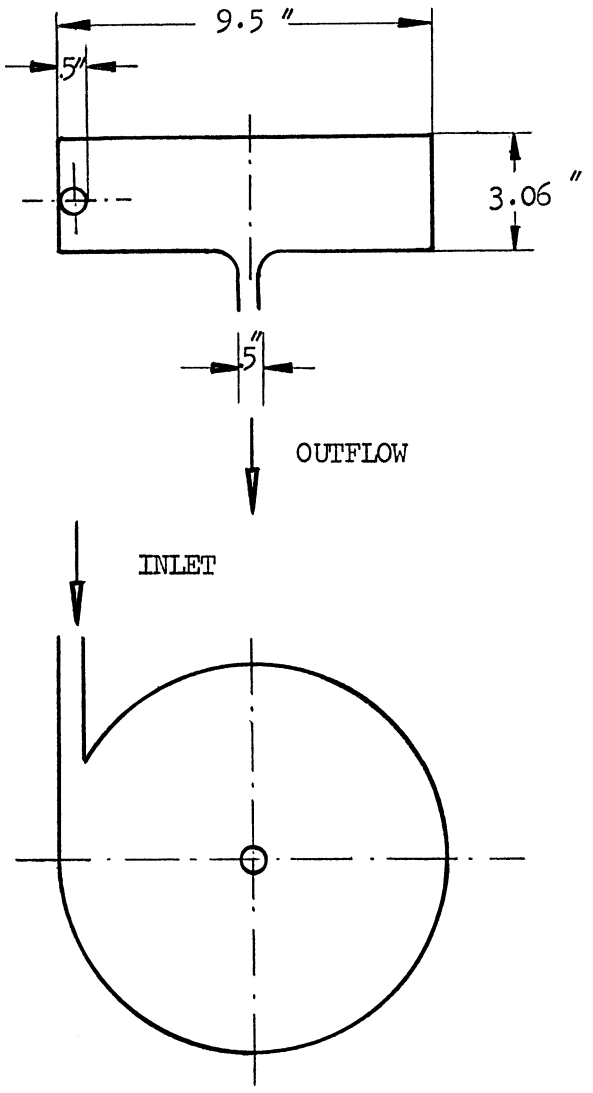

INVESTIGATED VORTEX CHAMBER CONFIGURATION

FIGURE 1

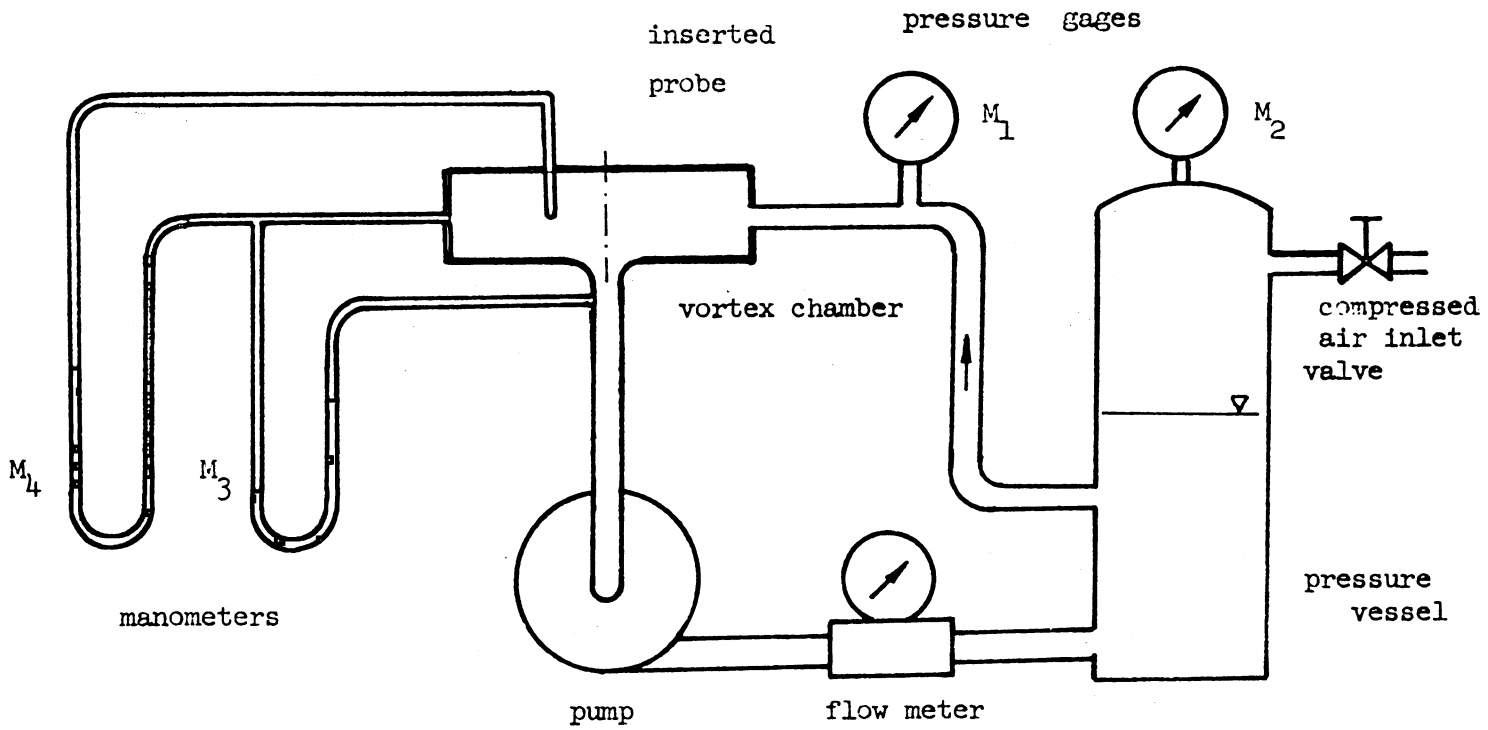

SCHEMATIC TEST STAND ARRANGEMENT

FIGURE 2

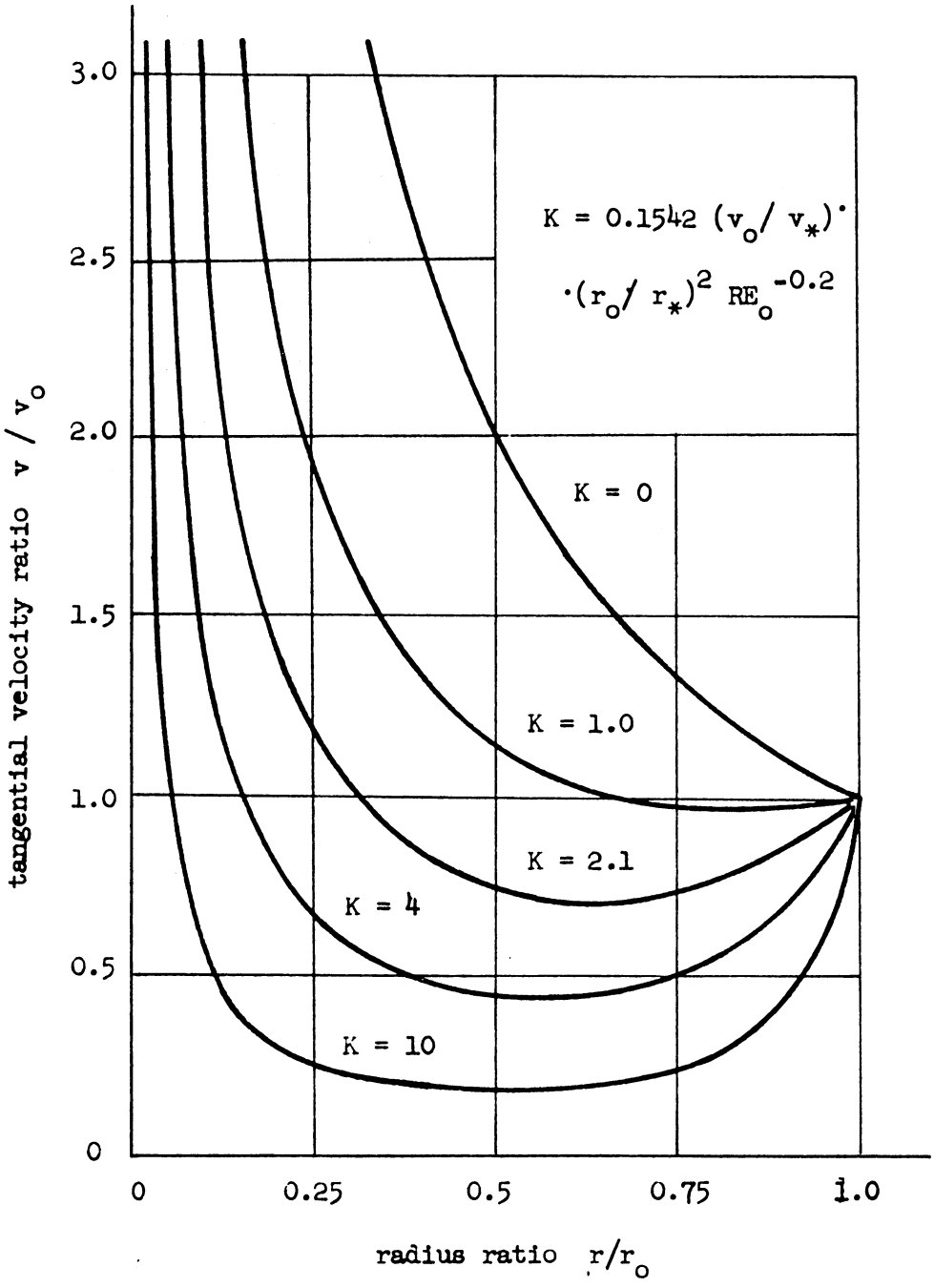

COMPUTED VELOCITY DISTRIBUTION

FIGURE 3

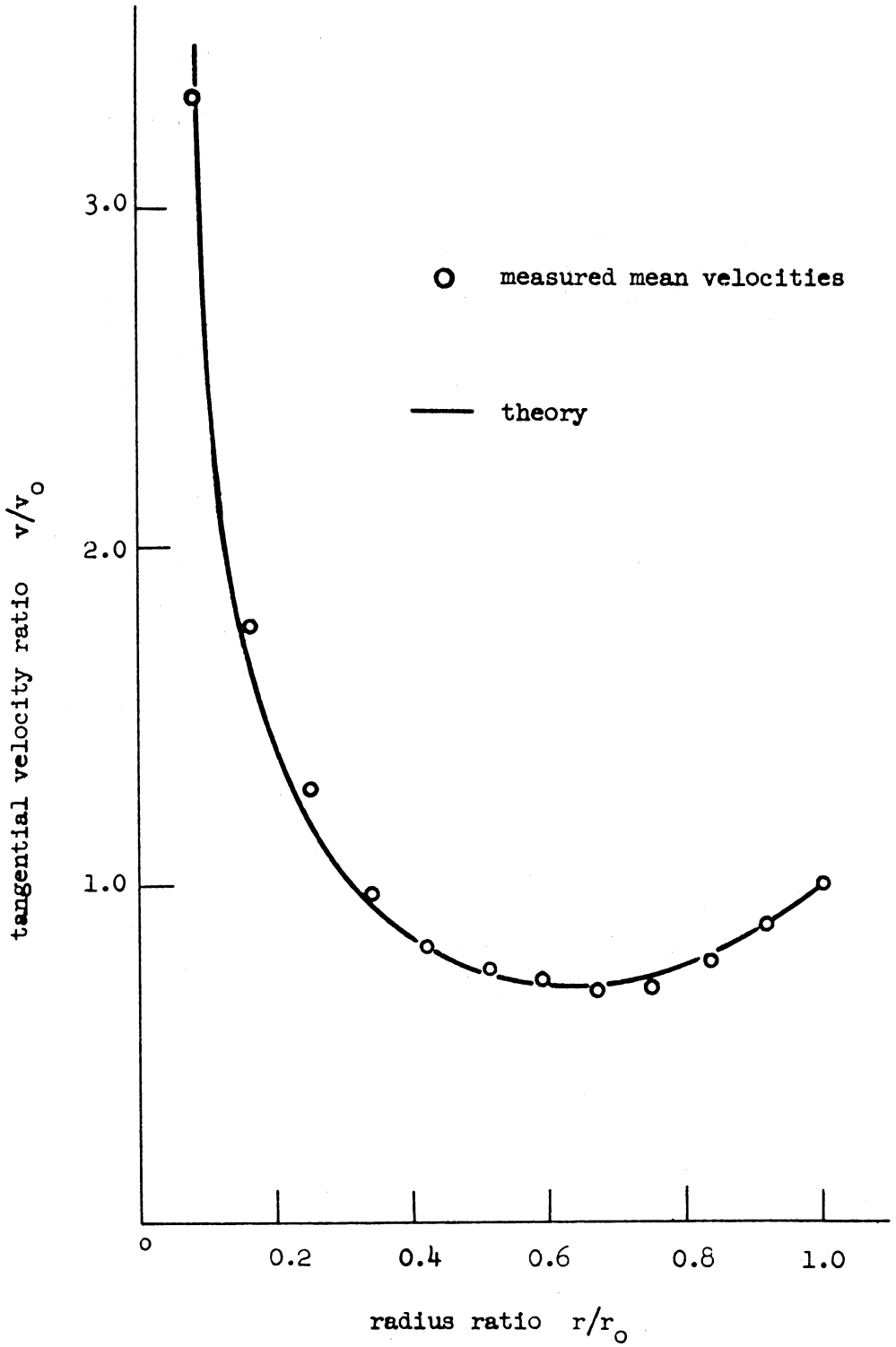

MEASURED VELOCITY DISTRIBUTION

FIGURE 4

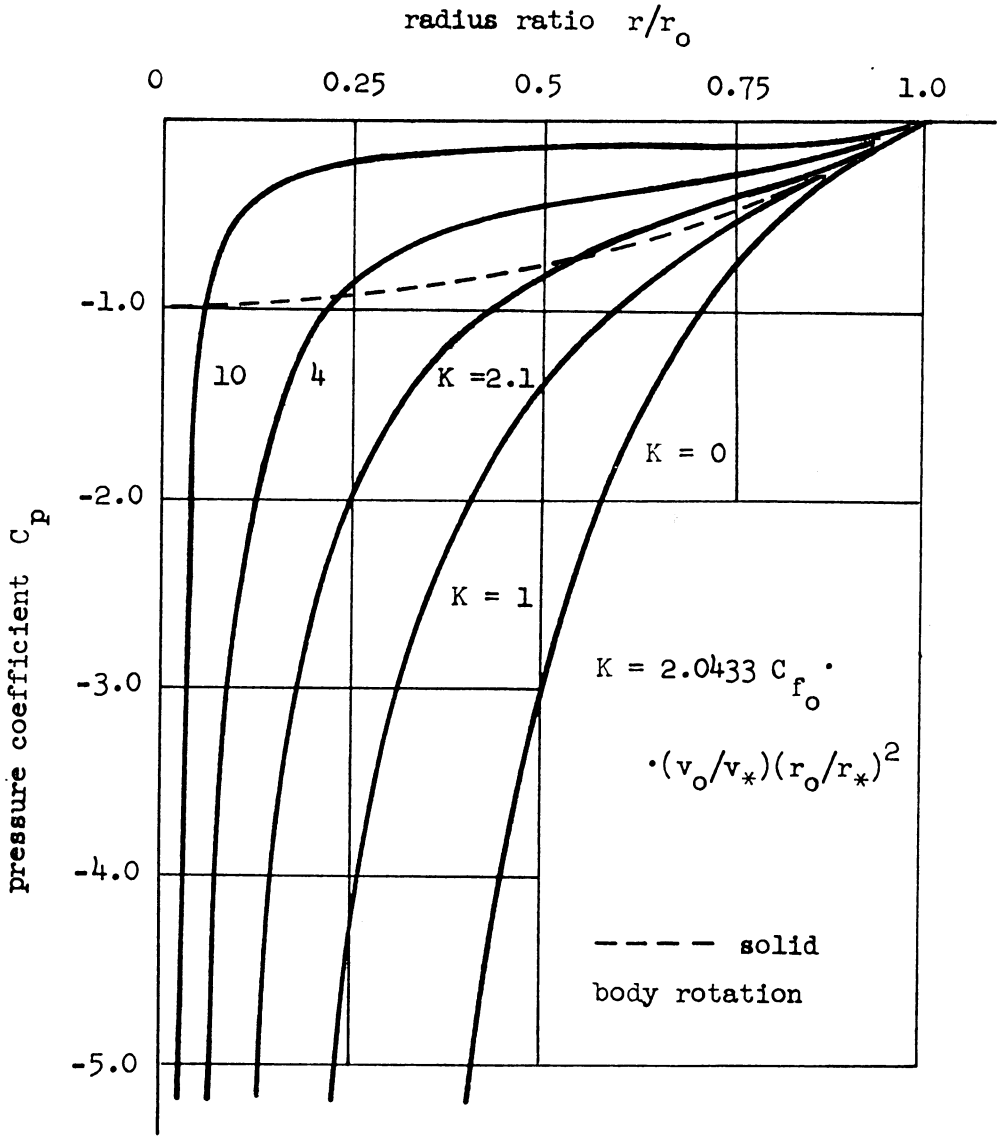

COMPUTED PRESSURE DISTRIBUTION

FIGURE 5

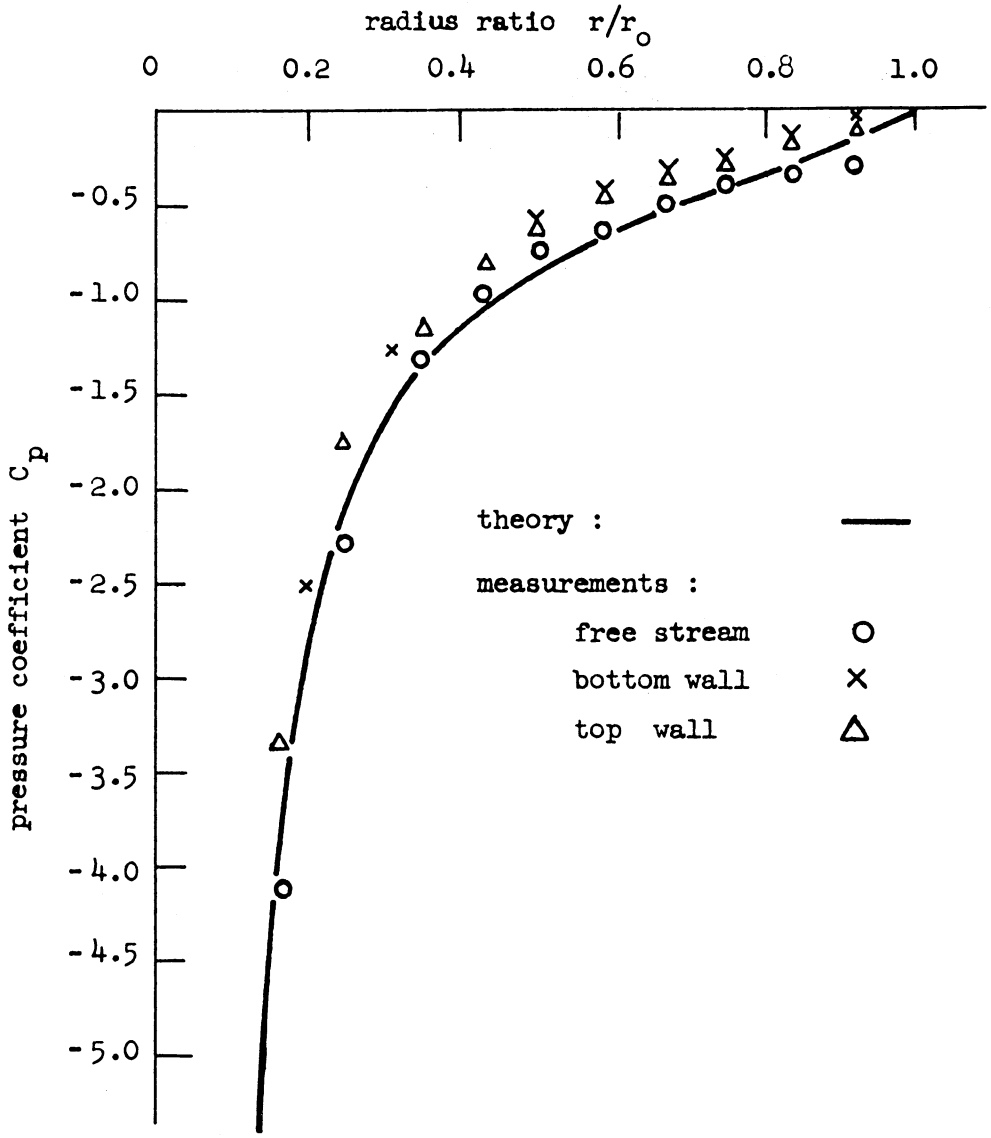

RADIAL PRESSURE DISTRIBUTION

FIGURE 6

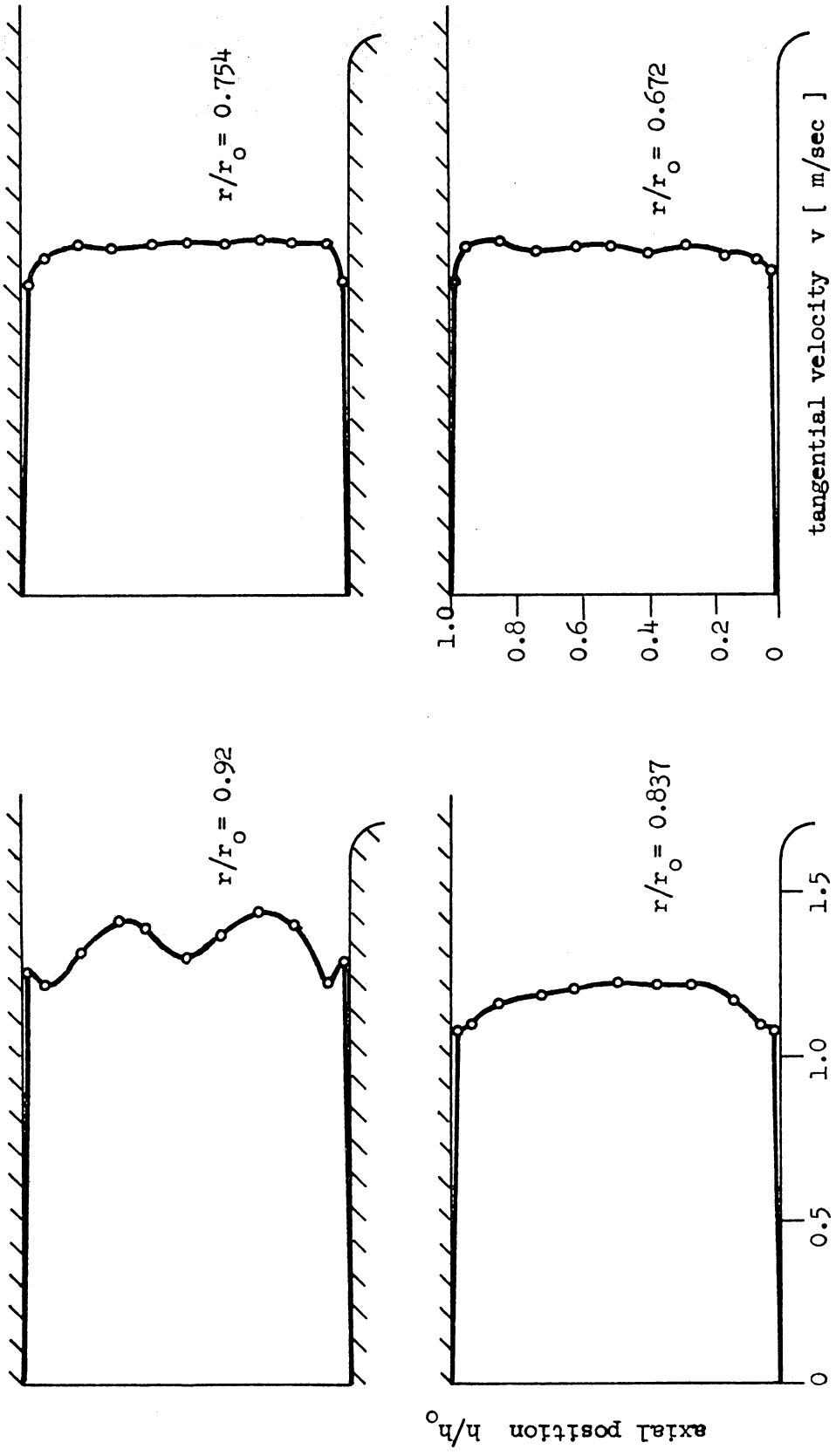

FIGURE 7 : MEASURED TANGENTIAL VELOCITY PROFILES

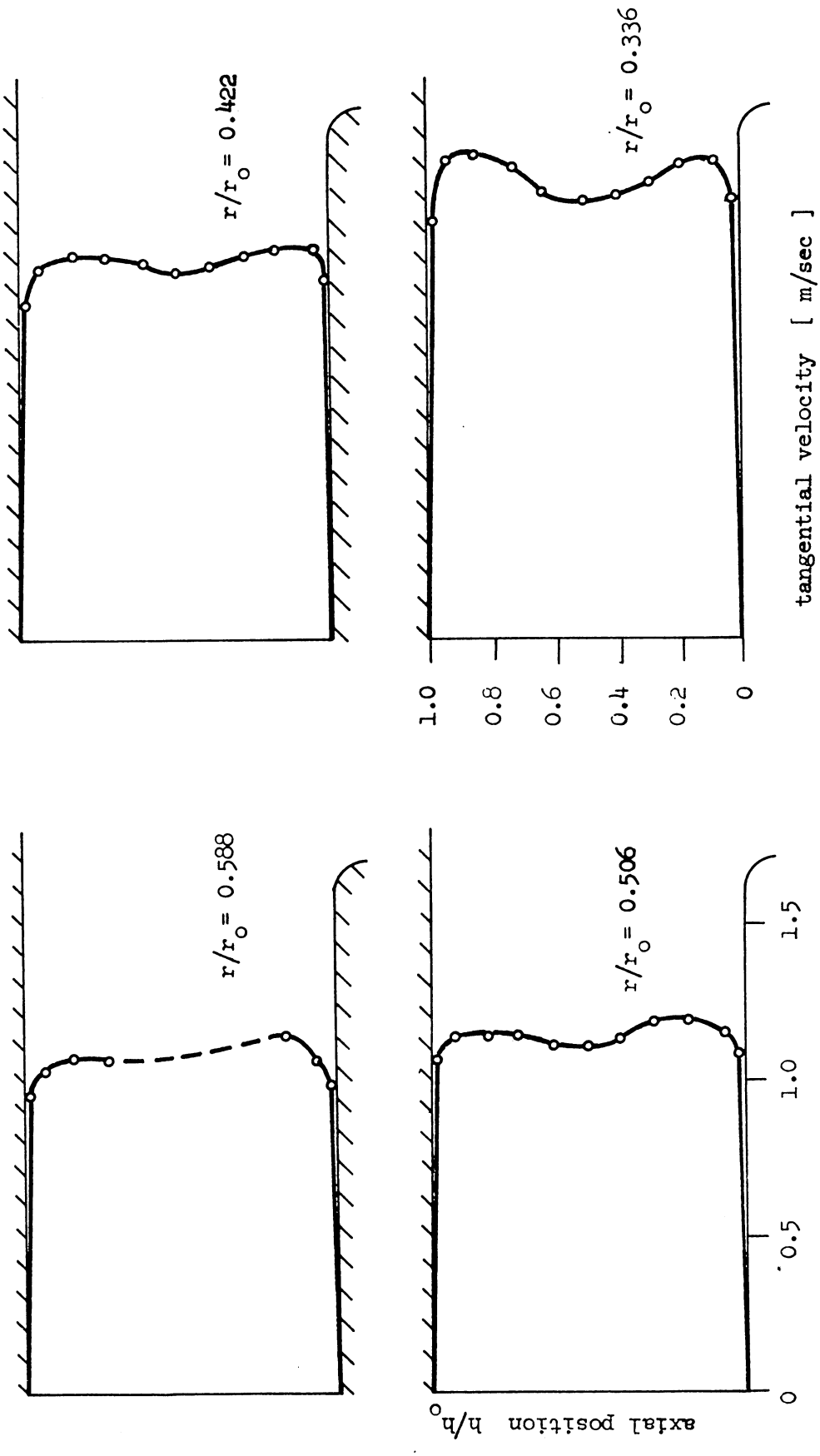

FIGURE 8 : MEASURED TANGENTIAL VELOCITY PROFILES

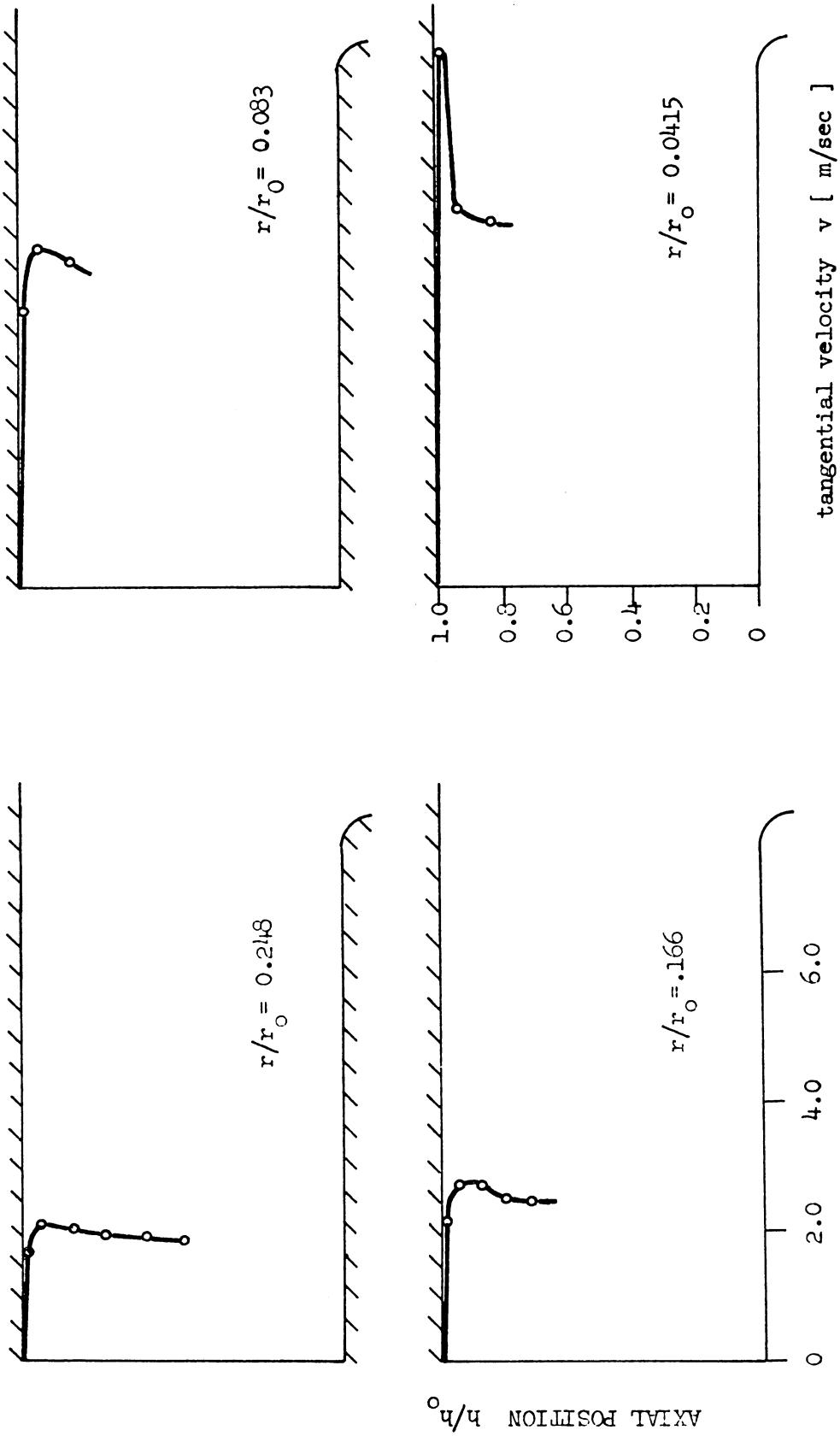

FIGURE 9 : MEASURED TANGENTIAL VELOCITY PROFILES

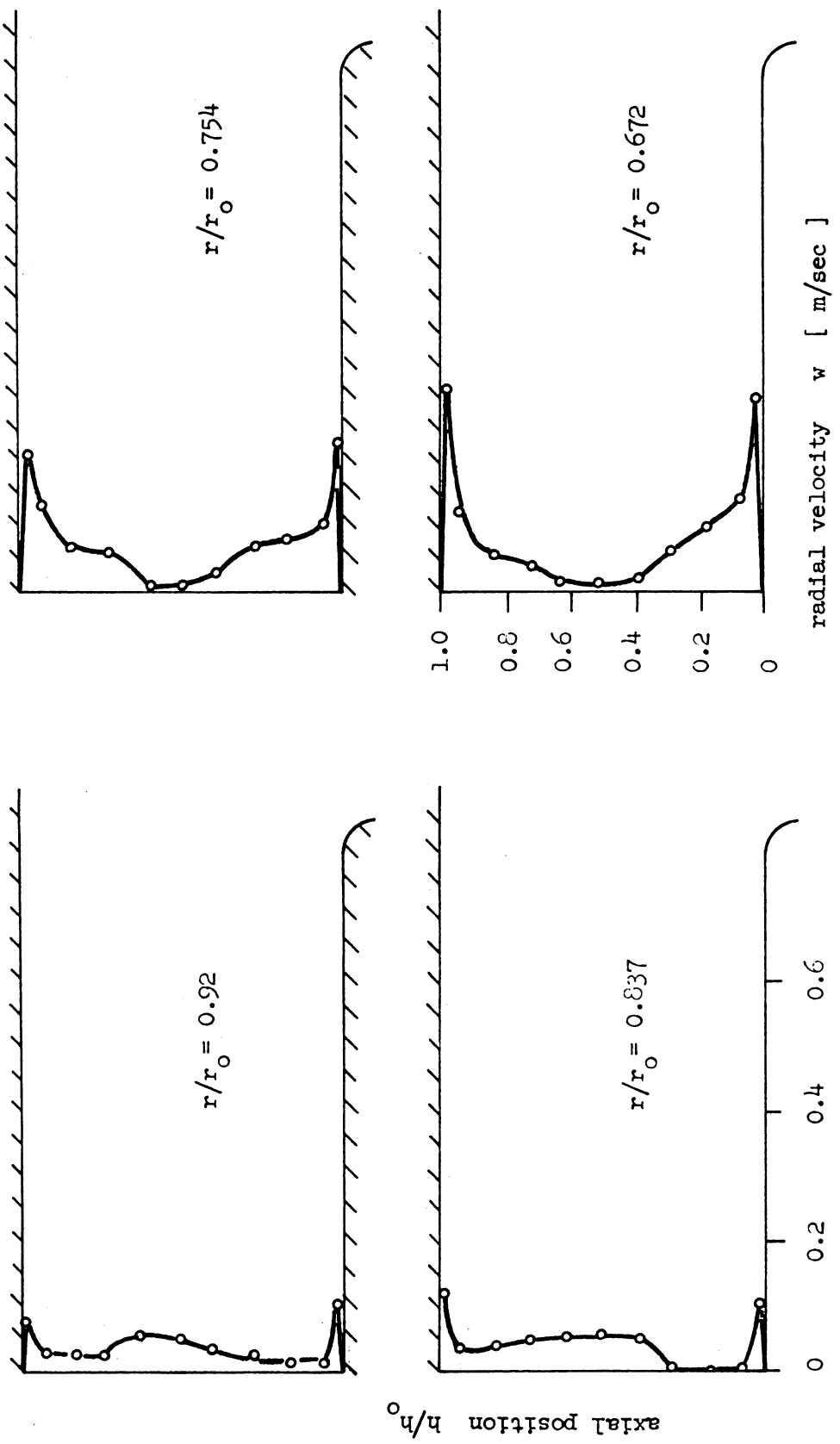

FIGURE 10 : MEASURED RADIAL VELOCITY PROFILES

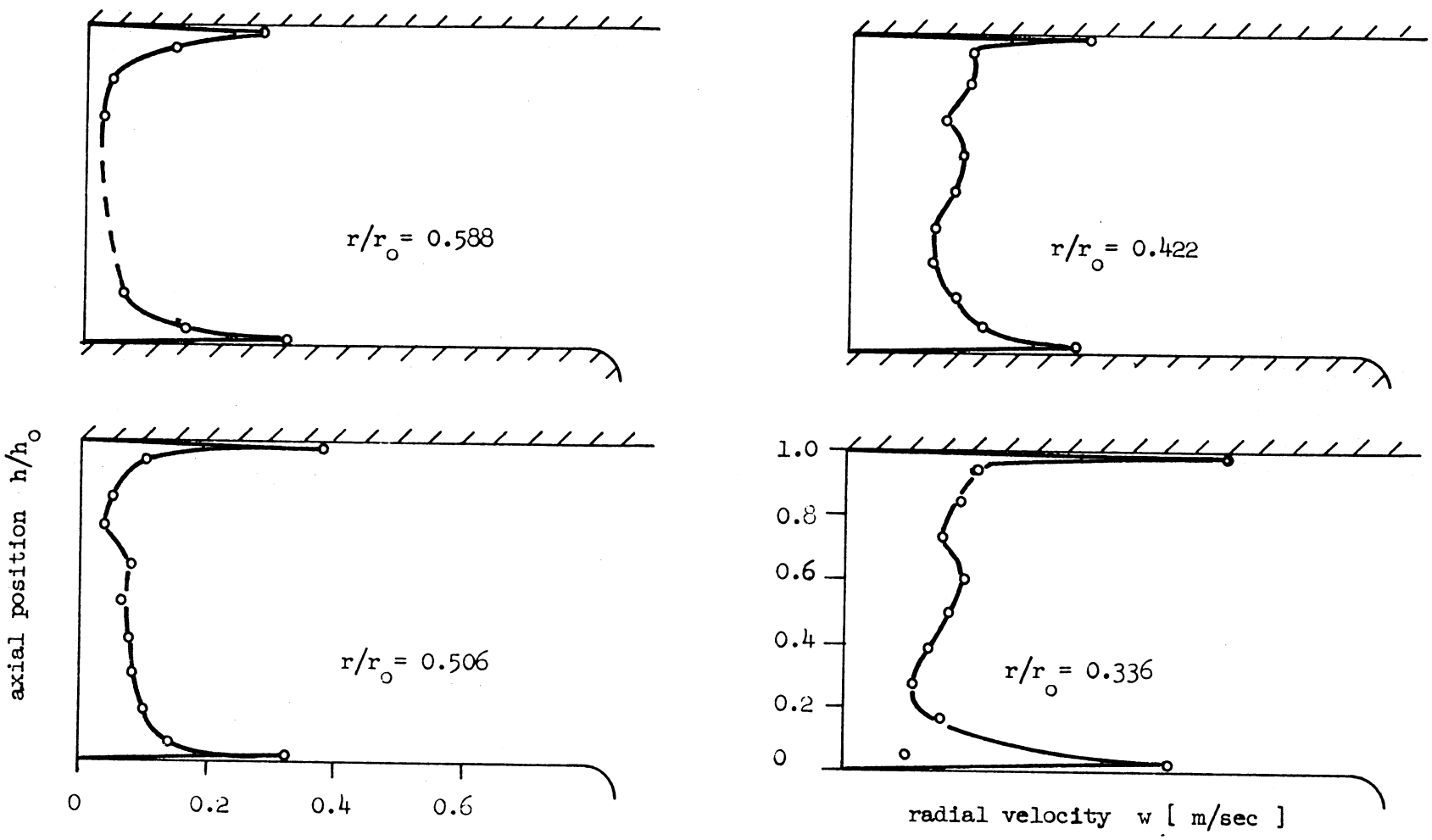

FIGURE 11 : MEASURED RADIAL VELOCITY PROFILES

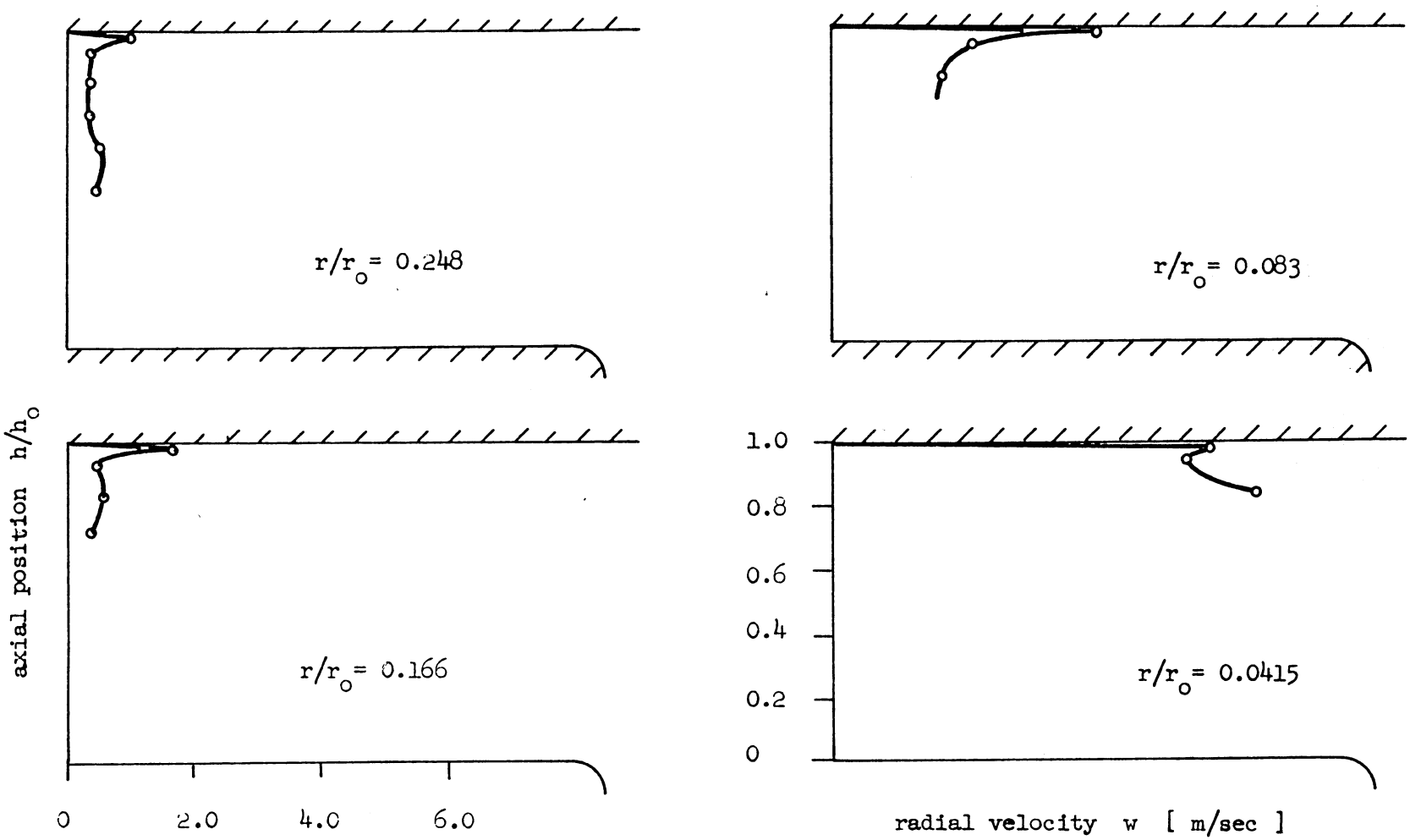

FIGURE 12 : MEASURED RADIAL VELOCITY PROFILES

APPENDIX

Brief Outline of the Numerical Integration Technique Used to Evaluate Equation (27)

Equation (27) gives the gradient $d C_p / d (r/r_o)$ of the wanted pressure distribution. The integration was begun at

$\xi = (r/r_o) = 1$ and $\eta = C_p = 0$.

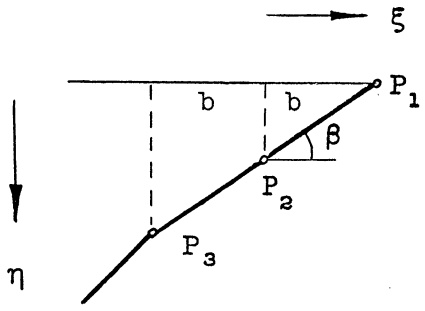

From the known point P_1 (ξ_1 , η_1) two new values of ξ were calculated by the relations

$$\xi_2 = \xi_1 - b$$

$$\xi_3 = \xi_1 - 2b$$

At the point P_2 (ξ_2) the gradient $(d\eta / d\xi)_2 = \tan \beta$ was determined. Then η_3 could be computed from

$$\eta_3 = \eta_1 - 2\, b \left(\frac{d\eta}{d\xi} \right)_2$$

By redefining $\xi_1 = \xi_3$ and $\eta_1 = \eta_3$ this whole procedure was repeated and a stepwise integration achieved. In the numerical analysis the step size b was chosen such that

$$b = 0.01 \, (r/r_o) \, .$$